Improving seismic image resolution in a carbonate fracture cave region: A case study

Naijian Wang[1], Xiao-Bi Xie[2], Mengchuan Duan[1], Daoshan Li[1], Ru-Shan Wu[2]*
1.Bureau of Geophysical Prospecting, 2.University of California at Santa Cruz

Summary

The carbonate reservoirs in Tarim Basin in Western China are characterized by their dissolution holes and karst caves along the faults in the limestone strata. They form a special type of "fault-karst" structure where faults and fractures are intertwined with dissolved pores and caves. The major challenges faced in this area are demands of high-resolution images and the generally weak seismic responses and low signal to noise ratios (SNR). This paper discusses major factors affecting image qualities and solutions to improve the resolution. Images from synthetic and real data sets are used to investigate the problem.

Introduction

The carbonate reservoirs in Tarim Basin are composed of karst faults and caves, unevenly distributed at depths 5.0-8.0 km. There are also numerous co-existed secondary structures including small cracks near the fault-cave systems. These are not only supplementary reservoir spaces, but also serve as connecting paths for adjacent faults and caves. They play significant roles in stable productions of reservoirs. Performing seismic survey and data processing to provide high resolution seismic image is vital for drilling and productions in reservoirs in Tarim Basin. On the other hand, these structures can be typically regarded as small-scale scatterers. Unlike signals reflected from layered targets, seismic responses from these small-scale structures tend to generate diffracted waves which often span wider angles in both incidence/scattering and azimuth directions. These signals are often weak and can easily be affected by different type of noises. Properly imaging these small-scale structures requires the data acquisition and processing system can cover wider incident/reflection angles, wider azimuth range and high source/receiver density. These may result in high cost in seismic survey and processing. Therefore, analyze parameters that will affect the image quality, properly balance the quality and cost is important in this region.

Researchers investigated related image problems from different aspects including diffraction tomography (Wu and Toksöz, 1987; Lin et al., 2018, 2019), illumination and resolution analysis (Xie et al., 2005; Yan and Xie, 2016), physical modeling studies (Xu, et al. 2014), and acquisition geometry (Feng et al., 2012; Wang et al., 2012). In this paper, we will analyze major factors related to the image resolution for small-scale targets in carbonate reservoirs in the Tarim Basin, and how to choose proper acquisition and processing parameters to improve the image resolution. As examples, images from both synthetic and real data sets from the Tarim Basin will be presented.

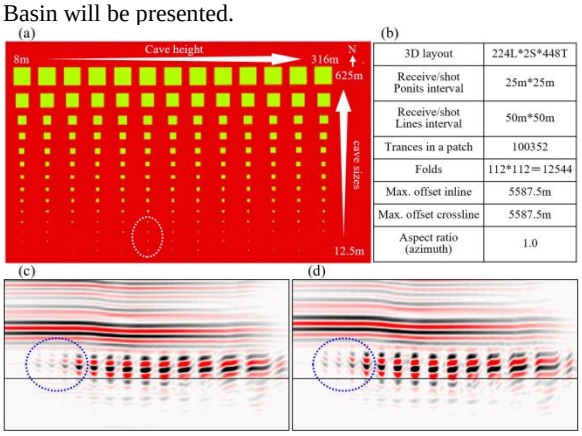

3D layout	224L*2S*448T
Receive/shot Ponits interval	25m*25m
Receive/shot Lines interval	50m*50m
Trances in a patch	100352
Folds	112*112=12544
Max. offset inline	5587.5m
Max. offset crossline	5587.5m
Aspect ratio (azimuth)	1.0

Figure 1: (a) A depth slice for a synthetic model with caves of different sizes. (b) Acquisition and image parameters. (c) and (d) Images using 25*25 and 12.5*12.5 m bin sizes.

Major factors that affect the image resolution with fault-cave structures.

The image resolution and bin sizes. The spatial resolution power of seismic data is mainly dependent on angle coverages and frequency. With given resolving power of data, choosing correct image bin size is important for imaging the fault-cave structure. Shown in Fig.1a is a model of 50 km^2, with karst caves of different sizes embedded at approximately 5000 m depth, overlaid by flat strata and a river sand body. The cave sizes gradually increase from 12.5 m to 625 m, and their heights increase from 8 m to 316 m. The 3D layout parameters in 1b are used for forward modeling and 3D Kirchhoff PSDM. Images using 25*25 and 12.5*12.5 m^2 bin sizes are shown in 1c and 1d. Obviously, big caves can be distinguished but smaller ones (circled by dotted lines) are hard to distinguish even using very small image bins. Fig.2 compares real 3D PSDM profiles with image bins of 30*30 and 15*15 m^2, where all large, medium and small caves are well imaged. The migration noise in latter case is lower due to the higher density of smaller bins.

The image resolution can also be demonstrated by how adjacent scatterers can be separated. Fig. 3a is a synthetic model, where groups of caves are embedded in a layered structure. The velocity is 4000 m/s and the dominant frequency is 25 Hz. The caves in different groups are separated by 1/8, 1/4, 1/3, 1/2, 2/3 and 1.0 λ, respectively, where λ is the dominant wavelength. In Fig 3b, additional depth variations are added to caves in each group. The

10.1190/segam2019-3215909.1

corresponding PSDM images are shown in 3c and 3d. The results reveal that, when adjacent caves are separated by less than λ/4, they cannot be properly separated due to wave interference. The example demonstrates that, when the resolving power of the data approaches its limit, further reducing the imaging bin size makes little benefit for image resolution. This is an important basis to avoid over-sampling when optimizing the image bin sizes.

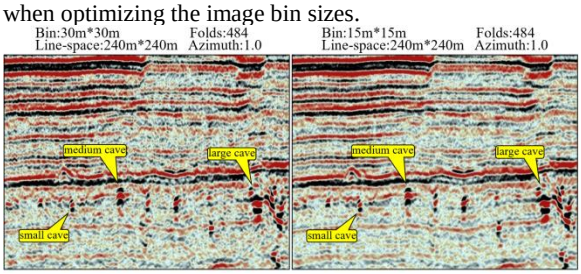

Figure 2: 3D PSDM profiles with different bin sizes

Wide-azimuth for fault-karst imaging and crack predicting. For small-scale karst fault-cave restructures, diffracted signals generated on these targets are weak but in very wide angles, both in dipping and in azimuth directions. Meanwhile, there are also numerous co-existing small cracks near the fault-cave systems. They play significant roles in drilling design and stable productions of the reservoir. Pre-stack crack prediction methods such as the OVT (offset-vector-tile) also rely on 3D data with wide dip and azimuth angle coverage and uniform distribution of attributes (Feng et al., 2012 and Xu et al., 2017). Therefore, it is important to image these crack-developed zones near faults and caves.

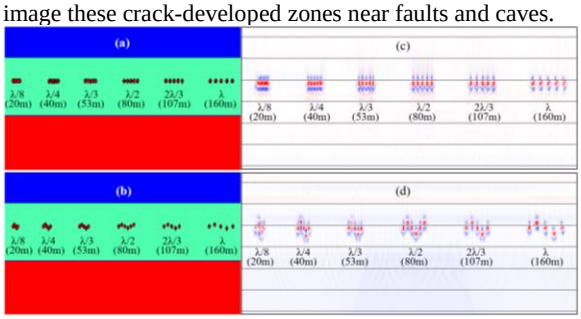

Figure 3: Synthetic models of multiple caves

Migration noise due to acquisition geometry and improper image bin sizes. As has been mentioned above, responses from fault-karst structures are dominated by weak diffracted signals, which are more easily to be affected by noises generated by acquisition footprint and improper imaging bin sizes. It is vital to eliminate effects from these noises and ensure the fidelities. Studies indicated that self-producing noises in migration is an inherent attribute of 3D layout. The regular shooting and receiving geometry often cause imaging conditions, e.g., offset and azimuth coverages in an area encircled by adjacent shooting and receiving lines unevenly distributed, which leads to periodic changes after migration and stacking. As illustrated in Fig. 4a-4d, using source and receiver line-spaces of 50, 100, 200 and 400 m, the offset/azimuth coverage in image bins in a sub area circled by source-receiver lines changing periodically. Larger line-space is often linked to large variations in offset /azimuth coverage, which cause serious acquisition footprint, particularly when the subsurface image bin is not properly designed according to the acquisition geometry. Fig.5 shows PSDM depth slices for a synthetic river sand body embedded in the velocity model of Fig.1 and using the four layouts shown in Fig. 4 for forward modeling. The results clearly show the migration noise associated with line-spaces.

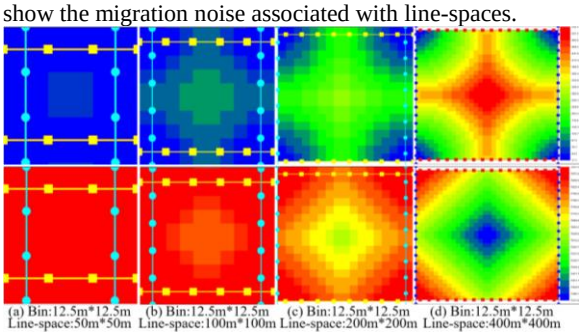

Figure 4: Variations of offset coverage related to the source-receiver line-space. Top: minimum and bottom: maximum offset distributions.

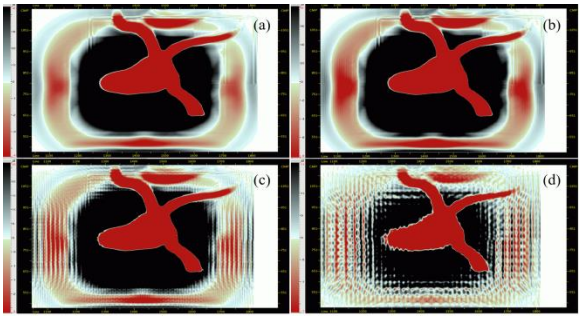

Figure 5: PSDM depth slices for a synthetic river sand body, (a) to (d) are correlated to line-spaces shown in Fig. 4

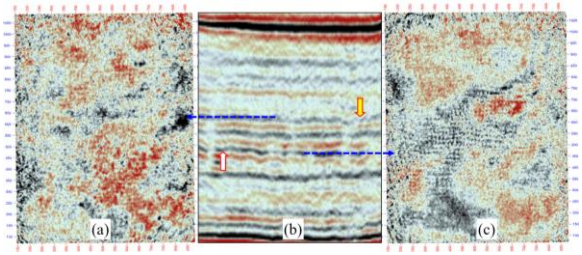

Figure 6: Migration noise in an real 3D data set

Shown in Fig.6 b is the vertical PSDM profile for a real 3D data set, 6a and 6c are depth slices of two layers with their depths indicated by arrows. It is clear that the left panel is a high SNR layer with weak migration noise, while the right panel is a poor SNR layer with strong migration noise.

10.1190/segam2019-3215909.1

Based on the above analysis, to obtain high quality images in carbonate fracture-cavity reservoirs, first there should be sufficient folds to generate high SNR data. Secondly, there should be enough azimuth and dip angle coverage ensuring the diffraction be properly received for both image and pre-stack crack predicting. The third, smaller line-space should be considered to reduce migration noise. Finally, proper image bin sizes should be used based on required spatial resolution and acquisition costs.

Illustrated in Fig. 7 is an example showing how to optimize 3D acquisition/processing parameters to trade off the quality and cost. The parameters of 3D layouts are labeled on the top of each panel. Shown in the middle panel is the result using small line-space and image bins. Both left and right panels are results obtained by using reduced densities in two different ways, with their field workloads and costs are basically the same. The left one uses larger line-space, small bin sizes, lower fold and coverage density; while the right one uses small line-space, larger bin sizes, higher fold and lower coverage density. All data sets are processed using the same velocity model and Kirchhoff workflow. The top and bottom rows in Fig. 7 are PSDM profiles and corresponding depth slices of RMS amplitudes along the fracture-cave layer. As expected, the result using intensive densities generates the best image quality and lowest migration noise, where small faults, caves and fractures (circled by dotted lines and indicated by arrows) are well imaged. On the left, although small image bins are used, due to the twice sparsely-sampled lines, the folds and coverage density are reduced by four times, resulted in heavy migration noise. The interpretation and identification of structures become difficult. On the right, the image bins are enlarged four times by twice sparsely-sampled, the coverage density is also reduced by four times. However, by keeping smaller line-space and high folds, it

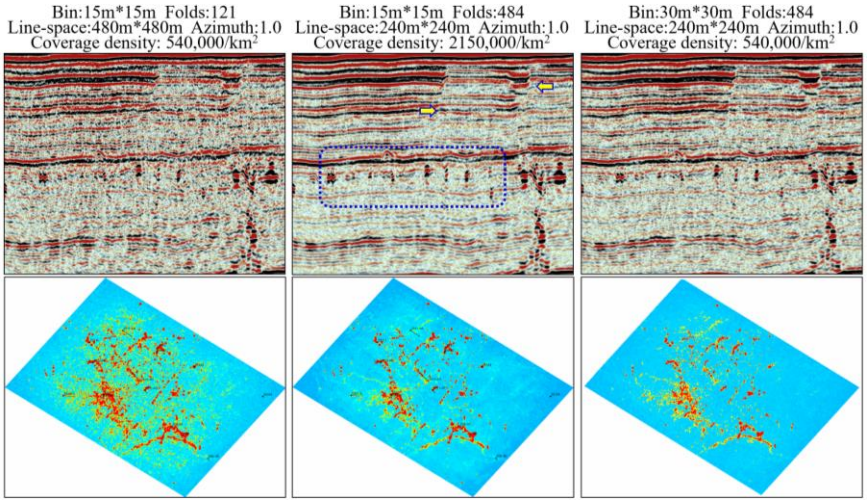

Figure 7: Comarisons of real data imaging with different 3D layouts

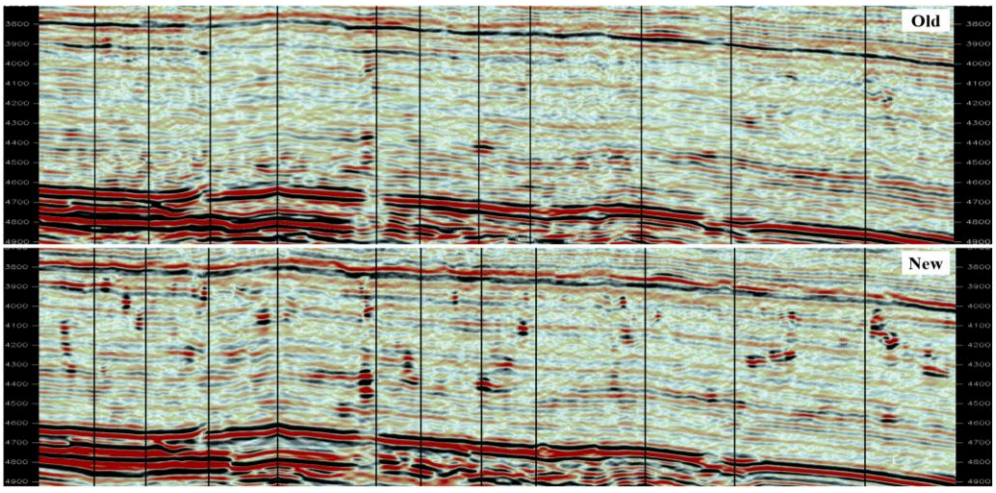

Figure 8: Comparison between migration profiles using the old (top panel) and new 3D (bottom panel) strategies.

10.1190/segam2019-3215909.1

still generates images of reasonable qualities, only costs slightly insufficiency in some details.

Real Data Examples

Previously, many low-density 3D seismic acquisitions were performed, and reservoir structures with medium to large-scale fault-karsts were investigated. However, due to the lower folds (60-84) and narrow azimuth (0.3-0.4) of these data sets, the image quality is unsatisfied and, in particular, the small faults and caves are not properly imaged, which limit the following interpretation and crack prediction. Recently, a number of high-density 3D acquisitions were carried out successively. The major enhancements are increasing fold numbers and coverage densities, reducing line-space and applying wide-azimuth. At the same time, the image bin sizes are kept unchanged or even slightly reduced. Fig. 8 and Fig. 9 compares PSDM profiles using the old and new strategies. The quality of the new 3D image is significantly improved with refined fault-cave structures and detailed cracks, which can effectively guide the design of horizontal well traces.

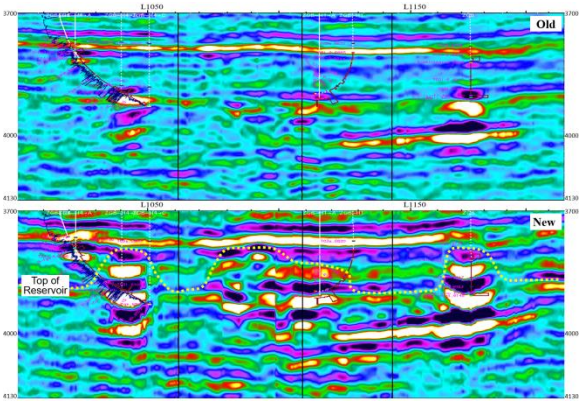

Figure 9: Comparison of enlarged portion of old/new PSDM

Another cost effective way to achieve high-density and wide-azimuth 3D data set is through "quasi full-azimuth" method, by applying an additional 3D acquisition along the direction perpendicular to an existing narrow azimuth 3D acquisition. Then integrate the prior and new 3D data to form a 3D data set with higher density and full-azimuth aperture. This makes full use of the exiting 3D data to obtain high density and wide-azimuth images with reduced cost.

Shown in Fig.10 is an example, where the upper row is for a pre-existing narrow-azimuth result, and the lower row is from the corresponding quasi full-azimuth result by combining an additional acquisition perpendicular to the existing one. Shown in column 10a are rose diagrams for azimuth coverages; column 10b are PSDM profiles over a cave along different azimuth directions; and column 10c are depth slices on the top of fault-karst structures. Because of the narrow azimuth and low folds, the previous 3D generated a poor image on the cave, particularly in the crossline direction (circled by dotted line in 10b). After adopting quasi full-azimuth method, the folds increased to 168, and the full azimuth are achieved within the entire migration aperture of 6 km. As a result, the cave is well imaged, the geologic features of the ancient river beds (indicated by arrows in 10c) and the boundaries of caves (circled by dotted lines in 10c) are more emphasized.

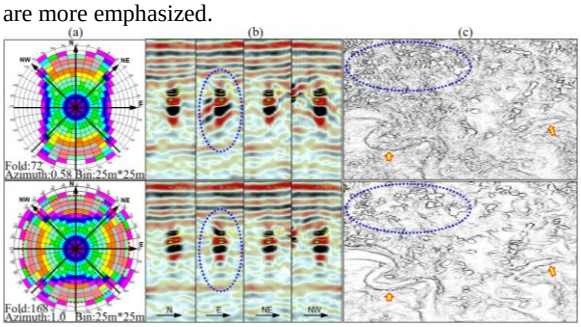

Figure 10: Comparison of 3D images after adopting the "quasi full-azimuth" method.

Discussions and Conclusion

The fracture-cavity carbonate reservoirs are characterized by small-scale scatterers with weak diffraction signals and low SNR along wide azimuth and dip directions. High-density (high folds) and wide-azimuth 3D data set is vital for ensuring high quality images demanded by both exploration and production. Given the acquisition density, layout with high folds and smaller line-space is preferred on improving image quality than that with smaller image bins and large line-space. Image bins should meet the needs of spatial resolution as well as avoid over-sampling. The acquisition footprint generated migration noise is an inherent attribute of 3D layout, with its strength correlated with the source/receiver line-space. Using small line-space can greatly reduce migration noise and improve the image fidelity. The frequency content of the signal and angle coverage jointly controls the wavenumber coverage, thus determines the spatial resolution of image. Based on illumination and resolution analyses, new techniques can be developed to further improve the image resolution in carbonate reservoirs with fault and cave structures.

Acknowledgments

The authors wish to thank Tarim Geophysical Method Research Institute for processing the data sets used in this case study. The assistances from the Tarim Oilfield Company and Research Institute of BGP for 3D data processing and interpretation are also appreciated. This study was partially finished at the WTOPI Research Consortium at UCSC.

10.1190/segam2019-3215909.1

REFERENCES

Feng, X. K., Y. F. Wang, X. J. Wang, N. J. Wang, G. C. Gao, and X. H. Zhu, 2012, The application of high-resolution 3D seismic acquisition techniques for carbonate reservoir characterization in China: The Leading Edge, **31**, 168–179, https://doi.org/10.1190/1.3686914.

Lin, P., S. P. Peng, J. T. Zhao, X. Q. Cui, and W. F. Du, 2018, Accurate diffraction imaging for detecting small-scale geologic discontinuities: Geophysics, **83**, no. 5, S447–S457, https://doi.org/10.1190/geo2017-0545.1.

Lin, P., S. P. Peng, J. T. Zhao, and X. Q. Cui, 2019, Diffraction separation and imaging using damped multichannel singular-value spectrum analysis: 81st Annual International Meeting Conference and Exhibition, EAGE, Expanded Abstracts, https://doi.org/10.3997/2214-4609.201901376.

Wang, X. S., X. Qian, and B. Li, 2006, The first Fresnel zone radius and lateral resolving power of seismic data: Progress in Exploration Geophysics, **29**, 224–248.

Wang, N. J., X. H. Liang, Y. Zhou, X. W. Liu, Y. F. Wang, X. Zhou, M. C. Duan, G. C. Gao, Y. H. Zhu, Y. Zhang, and Z. W. Mao, 2012, Inspiration of wide-azimuth 3D to oil and gas exploration in Tarim basin: Oil Forum, **31**, no. 2, 21–26.

Wu, R. S., and M. N. Toksöz, 1987, Diffraction tomography and multisource holography applied to seismic imaging: Geophysics, **52**, 11–25, https://doi.org/10.1190/1.1442237.

Xie, X. B., R. S. Wu, M. Fehler, and L. J. Huang, 2005, Seismic resolution and illumination: A wave-equation-based analysis: 75th Annual International Meeting, SEG, Expanded Abstracts, 1862–1865, https://doi.org/10.1190/1.2148066.

Xie, X. B., S. W. Jin, and R. S. Wu, 2006, Wave-equation-based seismic illumination analysis: Geophysics, **71**, no. 5, S169–S177, https://doi.org/10.1190/1.2227619.

Xie, X. B., Y. Q. He, and P. M. Li, 2013, Seismic illumination analysis and its applications in seismic survey design: Chinese Journal of Geophysics, **56**, 1568–1581.

Xu, H. X., C. G. Shen, B. Li, and W. X. Dong, 2017, Fault-karst carbonate reservoir prediction with comprehensive multi-attribute analysis: Oil Geophysical Prospecting, **52**, 158–163.

Yan, Z., and X. B. Xie, 2016, Full-wave seismic illumination and resolution analyses: A Poynting-vector-based method: Geophysics, **81**, no. 6, S447–S458, https://doi.org/10.1190/geo2016-0003.1.